

Article

# Relative Effect of Additional Solid Media on Bubble Hydrodynamics in Bubble Column and Airlift Reactors towards Mass Transfer Enhancement

Prajak Sastaravet <sup>1</sup>, Saret Bun <sup>2</sup> , Kritchart Wongwailikhit <sup>3</sup>, Nattawin Chawaloesphonsiya <sup>4,5</sup>, Manabu Fujii <sup>6</sup> and Pisut Painmanakul <sup>1,4,5,7,\*</sup>

<sup>1</sup> Department of Environmental Engineering, Faculty of Engineering, Chulalongkorn University, Bangkok 10330, Thailand; prajak.sas@hotmail.com

<sup>2</sup> Water and Environmental Engineering, Faculty of Hydrology and Water Resources Engineering, Institute of Technology of Cambodia, Phnom Penh 12156, Cambodia; saret@itc.edu.kh

<sup>3</sup> Center of Excellence in Particle and Materials Processing Technology, Department of Chemical Engineering, Faculty of Engineering, Chulalongkorn University, Bangkok 10330, Thailand; kritchart.w@chula.ac.th

<sup>4</sup> Research Unit on Technology for Oil Spill and Contamination Management, Chulalongkorn University, Bangkok 10330, Thailand; nattawin\_ch@hotmail.com

<sup>5</sup> Research Program in Remediation Technologies for Petroleum Contamination, Center of Excellence on Hazardous Substance Management (HSM), Bangkok 10330, Thailand

<sup>6</sup> Department of Civil and Environmental Engineering, Tokyo Institute of Technology, Tokyo 152-8552, Japan; fujii.m.ah@m.titech.ac.jp

<sup>7</sup> Research Network of NANOTEC-CU on Environmental, Department of Environmental Engineering, Chulalongkorn University, Bangkok 10330, Thailand

\* Correspondence: pisut.p@chula.ac.th; Tel.: +66-022-186-671

Received: 16 May 2020; Accepted: 16 June 2020; Published: 20 June 2020



**Abstract:** Many researchers have focused on multi-phase reactor development for improving mass transfer performance. However, solid particle addition in gas–liquid contactor for better oxygen mass transfer performance is still limited. Hence, this study aims to analyze the relative effect of different types of local solid media on the bubble hydrodynamic characteristics towards mass transfer enhancement in bubble columns (BCR) and airlift reactors (ALR). This was investigated by varying solid media types (ring, sphere, cylinder, and square), solid loadings (0%–15%), and superficial gas velocities ( $V_g$ ) ( $2.6$ – $15.3 \times 10^{-3}$  m/s) in terms of the bubble hydrodynamic and oxygen mass transfer parameters. The result showed that bubble size distribution in BCR and ALR with additional plastic media was smaller than that without media addition, approximately 22%–27% and 5%–29%, respectively, due to the increase of the bubble breaking rate and the decrease of the bubble rising velocity ( $U_B$ ). Further, adding media in both reactors significantly decreased the  $U_B$  value. Since media increased flow resistance, resulting in decreased liquid velocity, it can also be the moving bed to capture or block the bubbles from free rising. Therefore, oxygen mass transfer performance was investigated. The oxygen transfer coefficient ( $K_L a$ ) in BCR with solid media addition was enhanced up to 31%–56% compared to a non-addition case, while this enhancement was greater at higher solid loading due to its higher effective surface, resulting in a higher bubble break-up rate compared to the lower loading. In ALR, up to 38.5% enhanced  $K_L a$  coefficient was archived after adding plastic media over the non-addition case. In conclusion, ring and cylinder media were found to be the most significant for improving  $K_L a$  value in BCR and ALR, respectively, without extra energy.

**Keywords:** airlift reactor; bubble column; bubble hydrodynamic; mass transfer; solid media

## 1. Introduction

A bubble column reactor (BCR) is a multi-phase contactor device for transferring the gas in bubble form to contact with liquid. An airlift reactor (ALR), a type of BCR, is widely used in chemical and biochemical process industries. It is commonly designed as an internal-loop ALR (ILALR) and an external-loop ALR (ELALR). An ILALR generally presents as concentric tubes or split vessels which consist of riser and downcomer compartments. ILALR's advantages include simple operation, fewer maintenance requirements, simple construction, the absence of moving parts, and a high mass transfer rate [1]. In ILALR without a gas–liquid separator, different bubble hydrodynamic regimes can be observed through the bubble circulation between the riser and downcomer. Based on the study of We et al. [2], the flow regime is mainly based on the liquid velocity in the downcomer, which is divided into three classes. At low superficial gas velocity, the flow is in a bubble-free regime, which occurs when no bubble exists in the downcomer zone. By increasing the higher superficial gas velocity, the gas flow enters the transition regime, which bubbles partially and entrains into the downcomer zone. With continuous increasing superficial gas velocity, the flow enters the complete bubble circulation regime, in which the liquid circulation velocity becomes higher than the gas bubbles velocity in the downcomer. For the last case, the bubble was recirculated from downcomer to riser through the space below the split vessels.

BCR and ALR are multi-phase absorption reactors in which a gas phase is dispersed in the form of small bubbles into a liquid phase. These gas–liquid reactors have been extensively used in emission control process due to their simple construction, ease of operation, flexibility, and relatively high mass transfer efficiency. BCR and ALR performance is mainly affected by both gas and liquid dynamics, e.g., superficial gas velocity, operating pressure, air sparger design, gas hold-up, bubble diameter, liquid circulation, mixing level, adding suspended-solid phase, etc. Many researchers have investigated the extension of the bubble retention time for mass transfer period in the system with the modification of internals or additional structures. Bun et al. [3–5] enhanced the oxygen mass transfer coefficient ( $K_L a$ ) up to 97% compared to the regular reactor by adding slanted baffles in the riser compartment to increase the bubble retention time. Luo et al. [6] improved gas holdup and  $K_L a$  coefficient by providing sieve plates in the riser compartment. Nikakhtari and Hill [7] developed ALR by inserting nylon mesh packing in the riser, which resulted in a better  $K_L a$  coefficient compared to an unpacked one. Lukić et al. [8,9] also worked on ALR development by installing a self-agitated impeller in the riser to improve its performance.

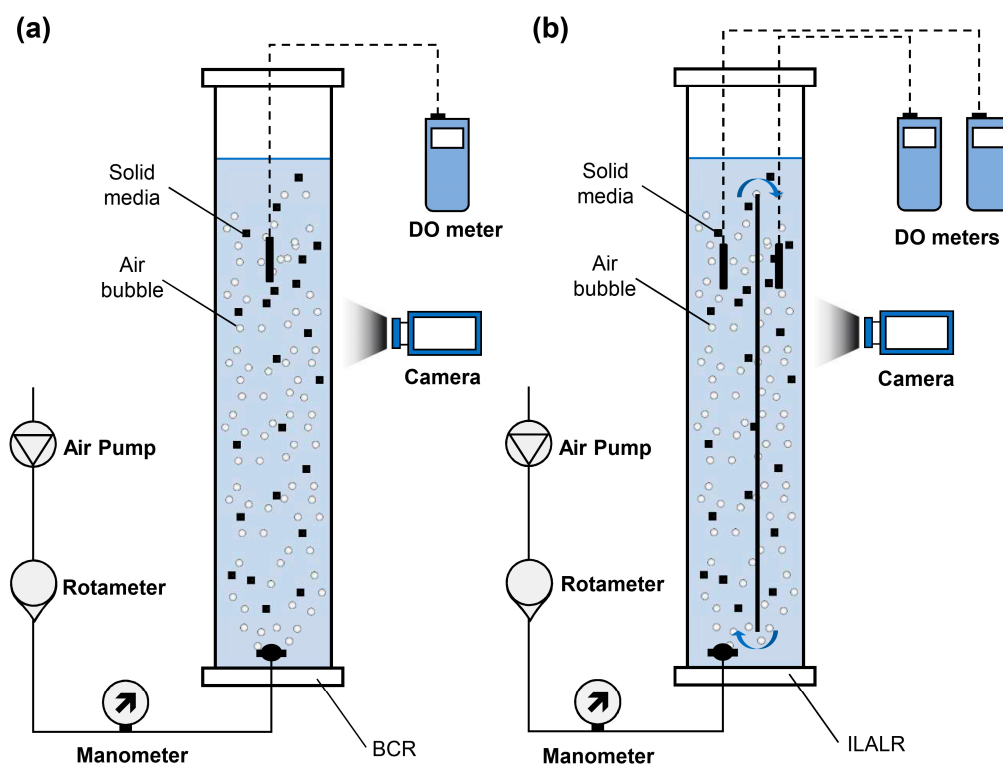
Beside ALR development for improving gas–liquid hydrodynamic characteristics and oxygen mass transfer performance through designing the efficient structures or internal configuration, the addition of a solid phase in gas–liquid reactors has also attracted much attention due to their numerous advantages over conventional reactors, including the excellent contact among the gas–liquid–solid phases which improve mass transfer rates. Recently, different studies have been applied to packed beds and moving solids in their gas–liquid reactor [10–12]. However, in-depth investigation of the relationship between particle characteristics and gas–liquid hydrodynamics or/and oxygen mass transfer performance is still required in order to understand the internal mechanism in the reactors as well as to extend the potential application of gas–liquid–solid contactors.

Hence, the objective of this study is to analyze the bubble hydrodynamic characteristics and mass transfer parameters after adding different physical properties of solid media in regular BCR and ALR. Four different polypropylene particles of solid media including ring, sphere, cylinder, and square were selected for investigating their relative effect on bubble hydrodynamics and oxygen transfer performance. These two main aspects include the parameters: bubble diameter ( $D_B$ ), bubble rising velocity ( $U_B$ ), bubble interfacial area ( $a$ ), overall volumetric mass transfer coefficient ( $K_L a$ ), liquid-side mass transfer coefficient ( $K_L$ ), and power consumption.

## 2. Materials and Methods

### 2.1. Experimental Set-Up

Two types of reactor, including regular BCR and ALR, which were constructed by clear acrylic as a cylindrical column, were used in this study. The bubble and airlift reactor are the same columns, with a 0.15 m inner diameter and a 1 m height, as shown in Figure 1, with a porous gas sparger at the column bottom for introducing air bubbles. The air was compressed by the air pump (Atman HP-12000) and controlled by an air valve and rotameter (DWYER®). A pressure gauge was also connected to determine the power consumption of the air pump. There was a free riser zone for the bubble column experimental test, while the additional acrylic plate was installed at a 3.18 downcomer-to-riser ratio ( $A_d/A_r$ ) to make the riser and downcomer compartments as a function of ALR. Additionally, a dissolved oxygen (DO) meter model HORIBA OM-51 was placed inside the column at the middle height for measuring the concentration of oxygen. A Basler high-speed camera was also set up around the middle height of the column to capture the bubble size distribution and rising velocity in both riser and downcomer compartments.

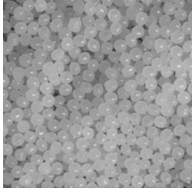
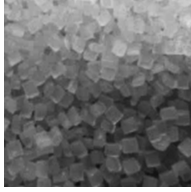


**Figure 1.** Experiment set-up of: (a) bubble column reactor (BCR), and (b) internal-loop airlift reactor (ALR).

### 2.2. Solid Particle Media

Various types of solid particles were added into the column test to investigate their relative effects on bubble hydrodynamic characteristics and mass transfer performance. Polypropylene media was selected for this experimental work due to their slightly lower density than water, approximately  $946 \text{ kg/m}^3$ , and uniform size, which may influence bubble distribution performance, floating and no accumulation in the bottle [13]. Four different polypropylene particles, i.e., ring, sphere, cylinder, and square sharps, were used for a comparative analysis in this study, as shown in Table 1. The solid loading concentration was ranged between 0% and 15% (v/v). Their physical properties are detailed in Table 1, including equivalent diameter, surface area, volume, and porosity.

**Table 1.** Physical properties and characteristics of solid media used in this study.

Parameters	Ring	Sphere	Cylinder	Square
Diameter (mm)	5.00	4.50	3.50	2.50
Surface area (mm <sup>2</sup> )	156.69	43.05	40.07	38.43
Volume (mm <sup>3</sup> )	49.48	26.56	29.35	17.69
Density (g/mm <sup>3</sup> )	$9.50 \times 10^{-4}$	$9.41 \times 10^{-4}$	$10.22 \times 10^{-4}$	$9.61 \times 10^{-4}$
Illustrated shape				
Image				

### 2.3. Bubble Hydrodynamics Analysis

#### 2.3.1. Bubble Diameter ( $d_B$ ) and Rising Velocity ( $U_B$ )

The bubble hydrodynamics were measured in both the BCR and ALR in terms of bubble diameter and rising velocity, using a photographic technique. The bubbles were originally captured by a high-speed Basler AG camera, model acA2000-340 km, with frame rate of 100 fps and 2 MP resolution. The observed bubbles had mainly ellipsoidal shapes characterized by the major axis,  $E$ , which represents the largest distance between two points on a bubble, and the minor axis,  $e$ , which represents the smallest length of the bubble [4]. Both axes were measured by ImageJ<sup>®</sup> software and the bubble diameter as the ellipsoid was calculated as following:

$$d_i = \sqrt[3]{E^2 e}, \quad (1)$$

The bubble hydrodynamic parameters of each experiment were randomly measured from 100–150 bubble samples. The bubble diameter ( $d_B$ ) was determined as the mean value:

$$d_B = d_{\text{Mean}} = \frac{\sum_{i=1}^n d_i}{n}, \quad (2)$$

where  $d$  is the diameter of each bubble and  $n$  is the amount of bubble samples selected for analysis. The bubble image processing used in this study is similar to the high-speed photography description of Xue et al. (2011) [14].

The bubble rising velocity ( $U_B$ ) was estimated by the rising motion distance of the bubble and its specific motion duration [4,15]. The placement time can be estimated from different captured frames and its frame rate set, while its distance can be observed with the reference meter, expressed as:

$$U_B = \frac{D}{t_{\text{frame}}}, \quad (3)$$

where  $D$  is the bubble spatial displacement between two frames and  $t_{\text{frame}}$  is the time between frames. The frame rate of 100 fps was set in this photographic technique.

### 2.3.2. Interfacial Area (a)

The interfacial area is the ratio between total air bubble surface and total volume including gas and solid phases. By assuming an air bubble presenting in a spherical shape, the interfacial area can be estimated by gas holdup, solid holdup, and bubble diameter [13], as expressed:

$$a = \frac{6}{d_B} \cdot \frac{\varepsilon_g}{1 - \varepsilon_g - \varepsilon_s}, \quad (4)$$

where solid holdup ( $\varepsilon_s$ ) can be determined using Equation (5):

$$\varepsilon_s = \frac{V_s}{V_g + V_l + V_s} \quad (5)$$

## 2.4. Mass Transfer and Power Consumption Estimation

### 2.4.1. Overall Volumetric Mass Transfer Coefficient ( $K_L a$ )

The  $K_L a$  coefficient is a principal parameter for evaluating the multi-phase reactor performance. The dynamic method was used in this study for defining the  $K_L a$  value [3,12]. The experiments were conducted with deoxygenation tap water. Sodium sulfite ( $\text{Na}_2\text{SO}_3$ ) was initially dissolved in order to remove dissolved oxygen (DO) in water through a chemical reaction. After the air was supplied, the DO level in the system was measured along time in both compartments using DO meters. The increasing DO profile in the function of time was therefore used for calculating  $K_L a$  coefficient, expressed as:

$$\frac{dC}{dt} = K_L a \cdot (C^* - C_t), \quad (6)$$

where  $C^*$  and  $C_t$  are saturated DO concentration and DO concentration at time  $t$ , respectively. Assuming liquid ideal-mixing,  $K_L a$  values can be determined from the slopes of  $\ln(C^* - C_t)$  as a function of time. Noted that the value of  $C^*$  can be estimated according to experimental temperature and pressure [16].

### 2.4.2. Liquid-side Mass Transfer Coefficient ( $K_L$ )

Theoretically, the volumetric mass transfer coefficient ( $K_L a$ ) is combined between the liquid side mass transfer coefficient ( $K_L$ ) and the bubble interfacial area ( $a$ ). Therefore, the  $K_L$  coefficient can be simply calculated by Equation (7):

$$K_L = \frac{K_L a}{a} \quad (7)$$

### 2.4.3. Volumetric Power Consumption

The power consumption was determined in terms of the volumetric power consumption ( $P/V$ ). It can be estimated in terms of volumetric gas flow rate ( $Q_g$ ) and total gas pressure drop ( $\Delta P$ ), as shown in Equation (8) [17]:

$$P/V = Q_g \cdot \Delta P/V \quad (8)$$

## 3. Results and Discussion

The results of this assessment study were mainly divided into two parts, i.e., the effect of additional solid media on bubble hydrodynamic characteristics and mass transfer performance. The investigated bubble hydrodynamic parameters include bubble diameter, bubble rising velocity, gas circulation rate, and bubble interbacterial area, while the  $K_L a$  coefficient,  $K_L$  coefficient, and power consumption were estimated as mass transfer parameters. It can be noted that this study investigated both regular BCR and ALR for comparative analysis.

### 3.1. Bubble Size ( $d_B$ )

Figure 2 presents the mean bubble diameter of all investigated solid media with the variation of superficial gas velocity ( $V_g$ ) and solid loading in BCR. Larger bubbles can be observed at higher  $V_g$ , regardless of additional media types (see Figure 2a). This is due to the bubble coalesce promotion at higher air-flow. The bubble distribution in the reactor with media was smaller than that without media, approximately 22%–27% on average. Wongwailikhit et al. (2018) [13] highlighted the three major influences of solid media addition on bubble hydrodynamics, i.e., increased bubbles breaking, increased bubbles coalescence, and decreased rising velocity. For this case, additional media was more likely enhancing the breaking rate than coalescence rate, which resulted in smaller bubbles with media. However, different relative effects were observed for various media types due to their effective properties. At lower gas flow ( $\leq 5.1 \times 10^{-3}$  m/s), no significant effect of the different additional media types on the bubble size was observed. The bubble diameter increased from  $2.81 \text{ mm} \pm 0.11 \text{ mm}$  to  $3.08 \text{ mm} \pm 0.08 \text{ mm}$  at  $V_g$  from  $2.6 \times 10^{-3}$  to  $5.1 \times 10^{-3}$  m/s, respectively. However, different effective performances were remarkable at higher gas flow ( $> 5.1 \times 10^{-3}$  m/s). Ring solid media resulted in the smallest bubbles, followed in order by sphere, cylinder, and square media, regardless of superficial gas velocity ( $V_g > 5.1 \times 10^{-3}$  m/s). These differences were possibly due to the different bubble break-up rates [13] and abilities for maintaining bubble size at higher gas flow [4] for each media. For instance, ring shape solid has both a higher bubble break-up rate due to its stronger force at the edges compared to edgeless solids and its ability to capture the bubbles inside avoiding bubble coalesce at higher gas flow [18]. However, this explanation cannot govern all solid cases studied since the sphere solid resulted smaller  $d_B$  compared to cylinder media. It is possibly due to the effect of particle size and effective surface (see Table 1). Hence, in this BCR, the particle size and surface effect may be stronger than the solid shape (edges) effect. Larger and higher surface solids could provide the better decouple performance compared to the smaller ones and result in minimizing the bubble coalescence in the reactor. As shown in the finding of Sarhan et al. (2018) [19], the slight decrease in coalescence efficiency with increasing particles size led to a decrease in bubble size.

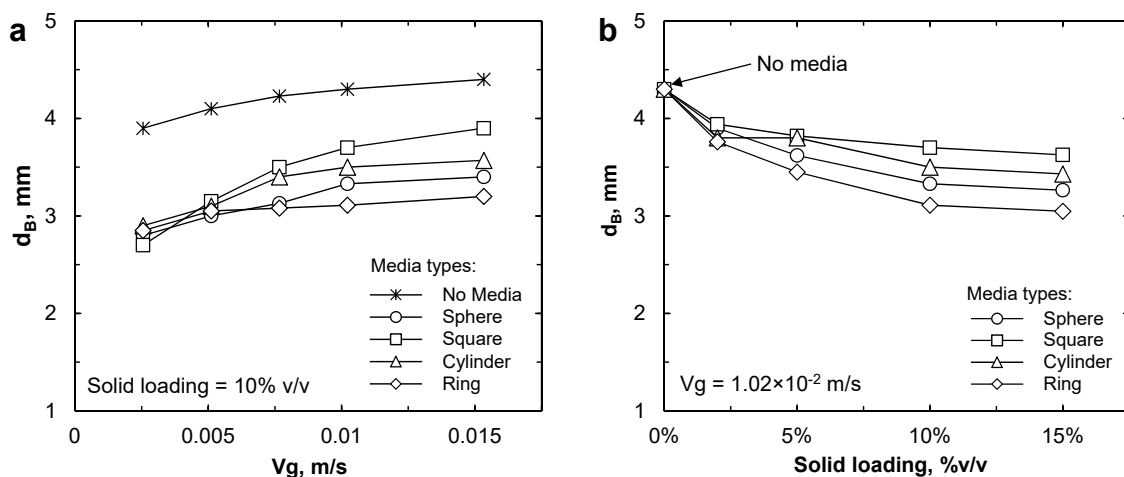


**Figure 2.** Mean bubble diameter ( $d_B$ ) in BCR for each solid media type with: (a) superficial gas velocity ( $V_g$ ) and (b) solid loading.

Different solid loadings were also investigated in terms of bubble diameter ( $d_B$ ) for each solid media in Figure 2b. A similar value of bubble diameter,  $3.85 \text{ mm} \pm 0.09 \text{ mm}$ , was initially observed at 2% solid loading for every solid media class. However, different trends were observed at higher solid loading ( $\geq 5\%$  v/v). Smaller bubbles can be obtained after increasing the solid loading percentage due to the enlargement of the bubble breaking rate through the higher amount of solid media in the gas–liquid–solid contactor. The ring solid still resulted in the smallest bubble diameter among the investigated media, followed in order by sphere, cylinder, and square solid media. For comparison,

the bubble size with ring solid addition was smaller than that with sphere, cylinder, and square solids by about 6%, 12%, and 16% on average, respectively. Moreover, increasing 5% to  $\geq 5\%$  solid loading could decrease approximately 10%  $d_B$  for ring, sphere, and cylinder solid media, while decrease only 4%  $d_B$  for square solid media. In summary, smaller bubbles can be obtained with additional solid media compared to non-addition, and bubble diameter decreased with the increase of solid loading for all investigated solid media. In terms of solid media comparison, the ring provided a higher bubble breaking rate among all employed solids, followed on order by sphere, cylinder, and square solids.

Figure 3 presents the mean bubble diameter of all investigated solid media with the variation of superficial gas velocity ( $V_g$ ) and solid loading in riser compartment of the ALR. A larger bubble size was obtained at a higher  $V_g$ ; in particular, no media was added due to the introduction of bubble coalesce at higher flow (see Figure 3a). The bubble in the ALR with media addition was smaller than that without media addition by around 5%–29% on average, possibly due to the increase of bubbles breaking and the decrease of bubble terminal rising velocity, as mentioned by Wongwailkhith et al. (2018) [13]. However, the tendency of bubble size change was different due to each solid media property. At lower flow ( $<10.2 \times 10^{-3}$  m/s), the cylinder media seems to be able to maintain a smaller air bubble, followed by the ring shape one. However, the ring media took this role at a higher flow. These differences can be explained through the different bubble break-up rates, e.g., ring and cylinder may have higher ability to capture the bubble and higher bubble break-up rate of the stronger edge force, respectively [4,13,18]. Additionally, different solid loadings of each solid media were also employed, as illustrated in Figure 3b. After adding solid media less than 5%, the square solid media provided the smallest bubble, followed by the ring and cylinder solid media. However, the ring and cylinder ones could maintain smaller air bubbles after increasing solid loading.

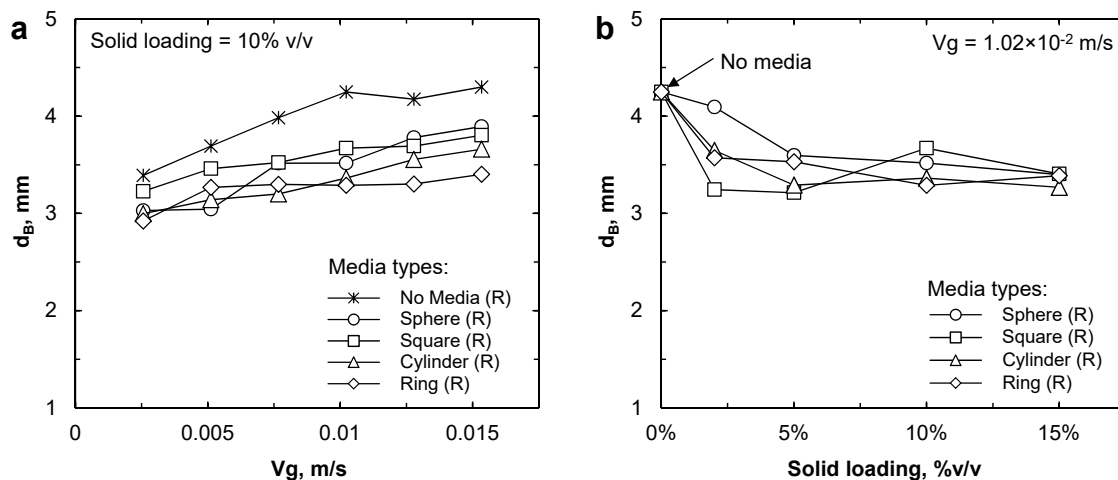


**Figure 3.** Mean bubble diameter ( $d_B$ ) in the riser compartment of ALR for each solid media type with: (a) superficial gas velocity ( $V_g$ ) and (b) solid loading.

The different bubble sizes in the BCR of each solid media addition can be observed, while the trend in ALR showed a similar  $d_B$  value. Therefore, other important parameters of bubble hydrodynamic characteristics should be examined. In the following sections, bubble rising velocity and interfacial area parameters were estimated for both reactors after adding each solid media.

### 3.2. Bubble Rising Velocity ( $U_B$ )

Beside bubble diameter, bubble rising velocity ( $U_B$ ) is another important parameter for the bubble hydrodynamic characteristics analysis of gas–liquid–solid reactors. Figure 3 showed the changes of  $U_B$  in the BCR for different solid media types by varying  $V_g$  and solid loading. The  $U_B$  increased with increasing  $V_g$ , but their increase tendency became weaker at higher  $V_g$  [20]. A lower  $U_B$  with different portions was noted from solid media addition compared to non-addition (see Figure 4a). However, gas

velocity almost has no influence on  $U_B$  when  $V_g$  exceeded  $1.02 \times 10^{-2}$  m/s, showing that the bubble rising velocity will be constant after increase until certain  $V_g$ . This result confirmed with finding of Zhang et al. (2005) [21], which reported that the solid particles increased the flow resistance of the system and resulted in a decrease in the liquid velocity. Further, the presence at a high concentration of solid media involves the moving bed capture or obstructs and blocks the bubbles from free rising. This effect especially relates with the ring particles, which had the highest surface area, leading to the highest drag force [10]. Additionally, the low  $U_B$  directly related to the small bubble. The ring solid showed the lowest velocity, 8.64–15.82 cm/s, compared to the other three solid media types and the non-addition case for  $V_g$  between  $2.6 \times 10^{-3}$  and  $15.3 \times 10^{-3}$  m/s. However, the  $U_B$  of sphere, cylinder, and square solids presented similar values between 14.37 and 18.84 cm/s.

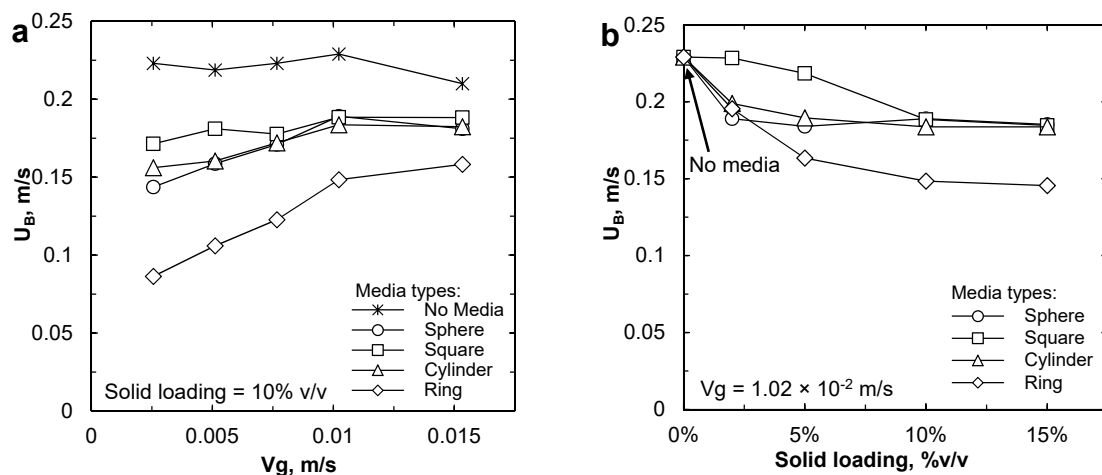


**Figure 4.** Bubble rising velocity ( $U_B$ ) in BCR of each solid media type with: (a) superficial gas velocity ( $V_g$ ) and (b) solid loading.

$U_B$  was also employed in terms of solid loading in Figure 4b at  $0.51 \times 10^{-3}$  and  $1.53 \times 10^{-3}$  m/s gas velocity. The  $U_B$  decreased with increasing solid loading with different tendencies based on each solid media property. The ring solid resulted in the lowest rising velocity, followed by cylinder and sphere solids, while the square one caused the highest velocity. The square solid presented in three patterns at  $\leq 2\%$ ,  $2\%–10\%$ , and  $\geq 10\%$  solid loadings. It seems that adding too little ( $\leq 2\%$ ) and too much ( $\geq 10\%$ ) square solid loading did not influence  $U_B$ , but by changing solid loading from 2% to 10%, the  $U_B$  decreased from 22.84 cm/s to 18.84 cm/s, respectively. A similar trend in  $U_B$  can be observed from adding cylinder and sphere solids. By increasing from 0% to 2% the cylinder and sphere solid loading, the  $U_B$  quickly decreased from 22.9 cm/s to 19.88 cm/s (cylinder solid) and to 18.9 cm/s (sphere solid). However, a slight decrease of  $U_B$  can be observed at higher loading ( $>2\%$ ). For the ring solid media, the  $U_B$  decreased with increasing solid loading, but its decrease tendency became weaker at higher solid loading, i.e., its decrease followed the second-order equation,  $U_B \approx 6.28x^2 + 1.46x + 0.23$ , where  $x$  is solid loading (%v/v) and  $U_B$  presents in m/s.

Figure 5 presents  $U_B$  in the riser compartment of ALR for different types of solid media added with the variation of  $V_g$  and solid loading. The pattern of  $U_B$  value increased between 7.19 and 18.42 cm/s with the increase of  $V_g$ , regardless of solid media types. The change of  $U_B$  value can be overall observed as two patterns between  $1.02 \times 10^{-2}$  m/s gas velocity. At  $V_g < 1.02 \times 10^{-2}$  m/s, adding ring and cylinder solids could slower the bubble rising velocity while adding square and sphere solids resulted in faster-rising velocity compare to the non-addition one (see Figure 5a). At higher gas flow ( $>1.02 \times 10^{-2}$  m/s), the pattern of square and no media addition were comparable, which are higher than the ring, cylinder, and sphere solid additions. From these results, it can be seen that between the BCR and the ALR, the  $U_B$  values in the ALR are significantly lower than that in the BCR. This might be due to the effect of the liquid recirculation flow pattern in the ALR resulting in

bubble break-up mechanism, as can be seen in the  $d_B$  value in the BCR and the ALR. Smaller bubbles tended to have lower rising velocity [22]. Moreover, every solid media added resulted in a positive performance in BCR through decreasing bubble rising velocity, mean increasing bubble retention time in a liquid system, especially the ring solid media due to its capability to capture the gas bubble inside. However, only ring and cylinder media could provide a lower bubble rising velocity in ALR compared to non-addition case.

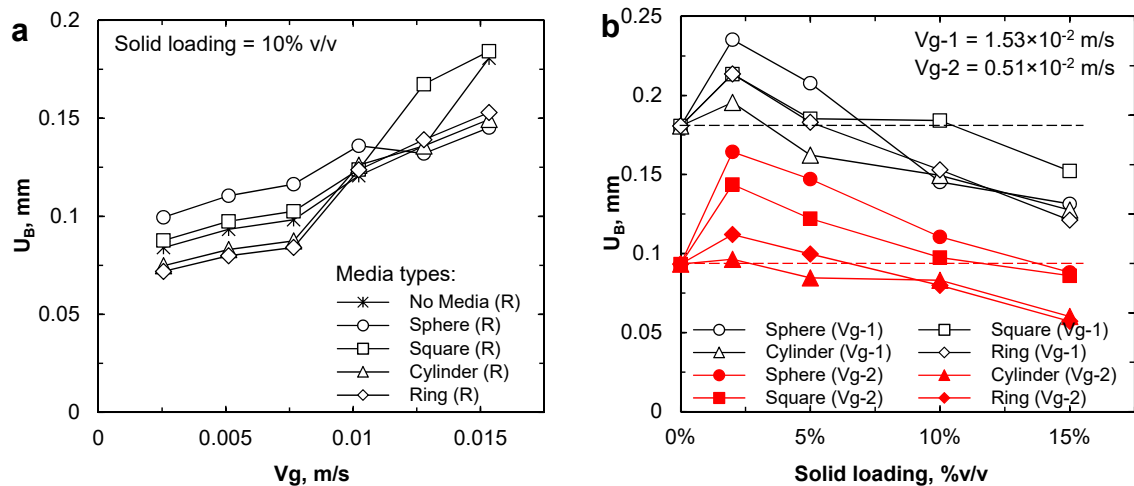


**Figure 5.** Bubble rising velocity ( $U_B$ ) in the riser compartment of ALR for each solid media type with: (a) superficial gas velocity ( $V_g$ ) and (b) solid loading.

For the analysis of the solid loading effect on  $U_B$  in ALR, it can be considered that the gas velocity at  $1.02 \times 10^{-2}$  m/s might be more complicated and unbeneficial to the analysis as it is the point of result pattern change. Therefore, the influence of solid loading in ALR was analyzed at  $0.5 \times 10^{-2}$  and  $1.5 \times 10^{-2}$  m/s superficial gas velocity, as illustrated in Figure 5b. For both  $V_g$  conditions,  $U_B$  was firstly increased after adding 2% solid loading before dropping back at higher solid loading (>2%). For low  $V_g$  ( $0.5 \times 10^{-2}$  m/s), only cylinder and ring solid media at 10%–15% could significantly decrease  $U_B$  compared to non-addition case. For higher  $V_g$  ( $1.5 \times 10^{-2}$  m/s), adding 5% cylinder media or more could provide a lower  $U_B$  value, while ring and sphere media were at 10% or more compared to the non-addition one. However, adding square media until reaching 15% was required to achieve its advantage on  $U_B$ .

In summary, adding solid media significantly decreased the bubble rising velocity in both reactors, and the slowest one can be obtained with the ring and cylinder types. In BCR, increasing solid loading could decrease rising velocity; however, its tendency turned to be weaker at higher solid loading, depending on the type of solid media, e.g., the observable point of significant decrease of square solid is between 2% and 10% while cylinder and sphere solids are at 2%, and the ring solid is less than 10%. In ALR, only ring and cylinder media with 10%–20% solid loading are able to decrease the bubble rising velocity, while another media, sphere type, can also be at higher  $V_g$  ( $>1.02 \times 10^{-3}$  m/s) and higher solid loading (15%). These findings can be used as the design criteria for the efficient gas–liquid–solid system with optimum bubble ring velocity as well as mass transfer performance.

### 3.3. Bubble Interfacial Area (a)

The low terminal rising velocity with solid media addition was directly associated with the smaller air bubble caused by the bubble break-up mechanism and the bubble captured with additional media. The condition with solid media possibly increased the bubble interfacial area (a) [23]. Therefore, this part aimed to determine bubble interfacial area in both reactors for selected solid media. Based on the results from previous parts, three solid media, i.e., ring, cylinder, and sphere types, at 5%–15%

were selected for this analysis as these conditions tended to have a potentially positive effect on bubble hydrodynamics and possible on mass transfer performance as well.

Figure 6 showed the result of the bubble interfacial area ( $a$ ) in both reactors for different operation conditions. It can be seen that the ring solid media added into the BCR resulted in highest interfacial area, regardless of superficial gas velocity, type of solid media, and percentage of solid loading. The highest performance of ring solid media can be explained due to its highest projected surface area resulted in highest drag force [13]. Besides the ring shape, the sphere solid media is another type that provided a high interfacial area, followed by the cylinder (Figure 6a). For the ALR, the cylinder media exhibited the highest value at 5% loading, followed by ring and sphere types. However, the cylinder and ring solid media presented similar value at higher solid loading, 10%–15%. It also can be noted that at the highest solid loading (15%) of the cylinder and ring media, the value of interfacial area reached the maximum at  $0.77 \times 10^{-2}$  m/s gas velocity (see Figure 6b). At high solids loading, higher gas flow ( $>0.77 \times 10^{-2}$  m/s) produced coarser bubbles and caused the bubble hydrodynamic characteristics to decay. This reverse effect was also found by Wongwailikhit et al. [13], adding too much solid loading resulted in the reverse effect for various types of solid media. Therefore,  $V_g \approx 0.77 \times 10^{-2}$  m/s can be suggested as the optimum condition if 15% of cylinder or ring media were used.

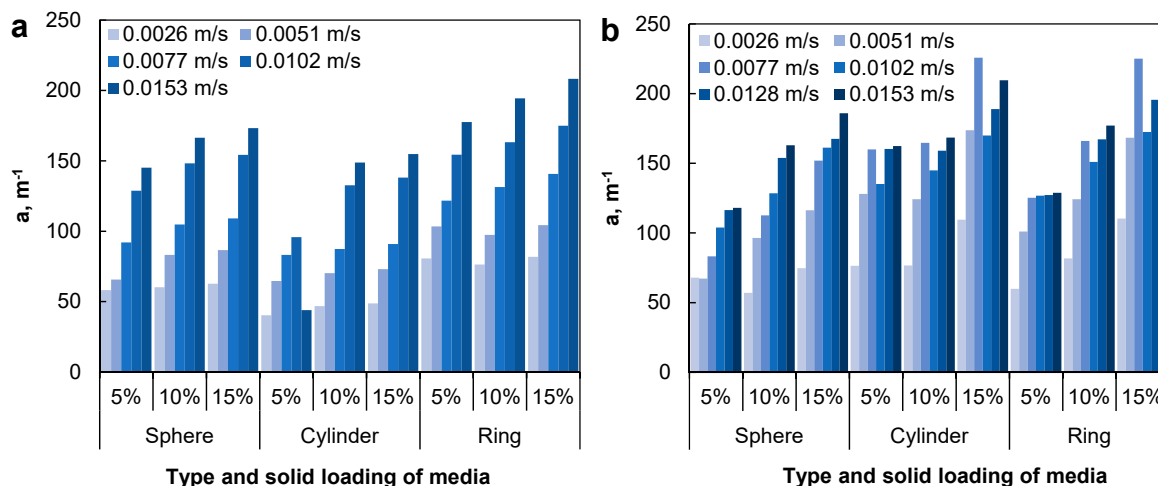


**Figure 6.** Bubble specific interfacial area ( $a$ ) with different solid loadings of each media type in: (a) BCR and (b) ALR.

### 3.4. Overall Mass Transfer Coefficient ( $K_L a$ )

Adding solid media into gas–liquid contactors resulted in the improvement of bubble hydrodynamics and possibly enhancing the oxygen transfer performance as well. Hence, the analysis of oxygen transfer parameters is necessary for projecting reactor performance as well as confirming the relationship between bubble hydrodynamics and mass transfer performance [24]. The  $K_L a$  coefficient in BCR is shown in Figure 7. The  $K_L a$  value increased speedily, corresponding to  $V_g$ , regardless of solid media types addition (see Figure 7a). Superficial gas velocity is the most significant parameter and a better  $K_L a$  coefficient can be acquired after increasing  $V_g$ , as previously found [25,26]. Adding solid media enhanced the  $K_L a$  coefficient up to 31%–56% compared to non-addition cases. This improvement is greater at higher solid loading, especially the ring shape media. It can be seen in Figure 7b that the possible effect of increasing solid loading on the  $K_L a$  value was observed as increasing solid loading, which caused higher effective surface and may also increase the bubble break-up rate compared to the lower loading. At 15% solid loading, ring media could rise in  $K_L a$  value from  $0.0201 \text{ s}^{-1}$  of the non-addition condition to  $0.0294 \text{ s}^{-1}$ , followed in order by the sphere ( $0.0270 \text{ s}^{-1}$ ), square ( $0.0264 \text{ s}^{-1}$ ) and cylinder ( $\sim 0.0261 \text{ s}^{-1}$ ). In brief, adding ring solid media significantly enhanced the  $K_L a$  value in BCR.

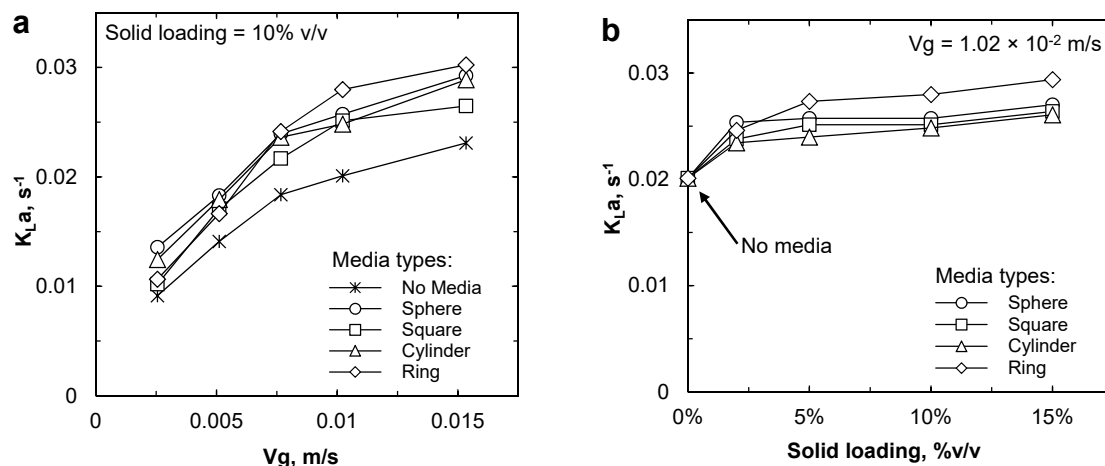


**Figure 7.** Overall mass transfer coefficient ( $K_{La}$ ) in BCR of each solid media type with: (a) superficial gas velocity ( $V_g$ ) and (b) solid loading.

For ALR, the result of the  $K_{La}$  coefficient from the riser compartment is illustrated in Figure 8. The performance of solid media presented in ALR can be classified into three patterns compared to the non-addition condition, i.e., cylinder, ring and square, and sphere types. Cylinder media showed the maximum value ( $0.009$ – $0.0284$  s<sup>-1</sup>) among the investigated media for the studied gas flow, and followed the power-trendline equation,  $K_{La(\text{cylinder})} \approx 0.525 \times V_g^{0.686}$  ( $R^2 \approx 0.98$ ). Secondly, ring and square solid media showed in similar trend with  $V_g$ , ranging between  $0.0075$  and  $0.0286$  s<sup>-1</sup>, and followed the power-trendline equation,  $K_{La(\text{ring/square})} \approx 0.763 \times V_g^{0.785}$  ( $R^2 \approx 0.98$ ). The last patterns and only the solid media provided a negative effect to lower the  $K_{La}$  value compared to the non-addition case, and the sphere media showed a slight increase from  $0.0066$  to  $0.0162$  s<sup>-1</sup>, which is about 20% on average less than without the media added. Hence, sphere solid media was not suggested to apply in ALR toward mass transfer enhancement, only the cylinder, ring, and square are possible. This poor performance of the sphere particle is possibly due to its low density and high affinity to interface of the bubble among the investigated solid particles. Lower density has a higher terminal velocity [13] and results in higher  $U_B$  value (see Figure 5); consequently, lower  $K_{La}$  value will be obtained. This similar finding was also described by Ferreira et al. (2010) [27]: a significant decrease in mass transfer can be observed from the use of solid particles with low density and high affinity to the bubble interface. However, this mechanism may not significantly be observed in BCR. It might be related to the liquid velocity after maintaining a constant  $V_g$  and cross-sectional area of ALR divided into two compartments. Higher liquid velocity in the ALR will significantly lead to faster terminal velocity of the sphere solid as well as  $U_B$ , compared to the one in the BCR.

Moreover, their effect on  $K_{La}$  coefficient was also specified at different solid loadings for every solid media. Three trends of the result were also remarkable. Firstly, the  $K_{La}$  value increased with the higher amount of cylinder solid media. However, its tendency became constant at higher solid loading (>10%). Secondly, increasing solid loading only did not significant effect the  $K_{La}$  values of the ring and square media addition, approximately  $0.0209 \pm 0.0012$  s<sup>-1</sup>. Lastly, the sphere media decreased after increasing the amount of solid loading. Based on these results, it can be summarized that cylinder, ring, and square media can be selected for improving oxygen mass transfer in ALR with the gas flow around  $1.28 \times 10^{-2}$  m/s. However, the optimum solid loading for cylinder and ring/square are 10% and 5%, respectively.

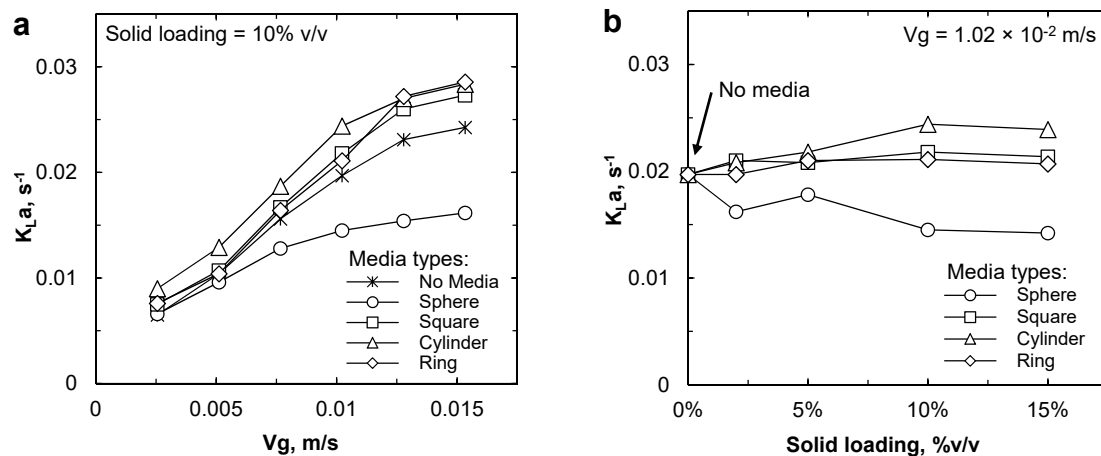


**Figure 8.** Overall mass transfer coefficient ( $K_L a$ ) in the riser compartment of ALR for each solid media type with: (a) superficial gas velocity ( $V_g$ ) and (b) solid loading.

In conclusion, adding solid media in a multi-phase reactor enhanced the oxygen mass transfer coefficient ( $K_L a$ ) performance compared to the non-addition case with different tendencies, based on the characteristics of each type. Ring solid media were defined as the most significant media for improving the  $K_L a$  value in BCR among the four examined types, while the other three presented a similar trend. Moreover, higher solid loading resulted in better oxygen transfer behaviors. Additionally, the cylinder solid media was found as the most effective media for enhancing the  $K_L a$  coefficient in ALR, while the ring and square media presented a similar performance. A 10% cylinder and 5% ring or square should be applied for optimizing the system operation. These defined conditions are the design criteria for applying these solid media in BCR and ALR to obtain better oxygen transfer performance without extra energy.

### 3.5. Liquid-Side Mass Transfer Coefficient ( $K_L$ )

The liquid-side mass transfer coefficient ( $K_L$ ) was also estimated in this study for additive information. It was calculated using Equation (7), which was mainly based on the result of mass transfer,  $K_L a$  coefficient, and bubble hydrodynamics, specific interfacial area. Figure 9 showed the values of the estimated  $K_L$  coefficient for different types of solid media in both reactors. Based on Figure 9a of BCR, the  $K_L$  value decreased with the increase of  $V_g$ , except for ring solid media. As mentioned, it was calculated from the experimental result that the lowest  $K_L$  of the ring media is caused by its highest value in the interfacial area parameter among other media classes (see Figure 6a). The tendency of other media types, e.g., sphere and cylinder media, was also significantly related to their bubble interfacial area values. The value of  $K_L$  in ALR is much lower than that of BCR due to the significant difference in bubble hydrodynamic parameter, mainly presented by interfacial area value (see Figure 6b). At lower gas flow ( $\leq 0.77 \times 10^{-2}$  m/s), ring media showed the lowest  $K_L$  value, while sphere media was at higher flow due to the tendencies of  $K_L a$  and interfacial area values.

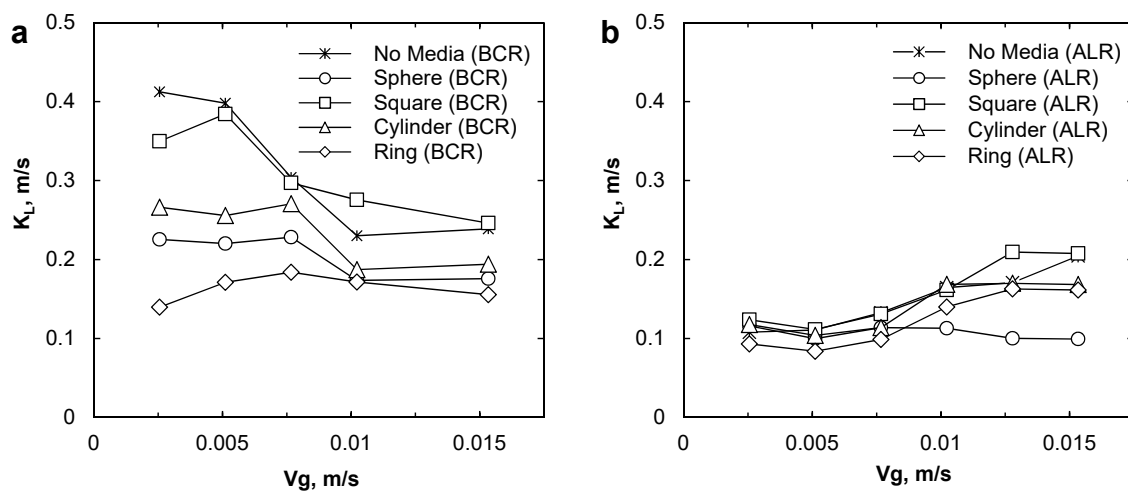


**Figure 9.** Estimated liquid-side mass transfer coefficient ( $K_L$ ) coefficient with different solid media types and 10% loading in: (a) BCR and (b) ALR.

### 3.6. Power Consumption

Variations of specific power consumption with 10% solid particle concentration at  $1.02 \times 10^{-2}$  m/s gas flow are shown in Figure 10. A higher  $P/V$  value resulted in better  $K_L a$  coefficient performance, as expected. The  $K_L a$  value ranged between 0.0065 and  $0.0302 \text{ s}^{-1}$  and was achieved by providing  $P/V$  from 2.2 to  $9.6 \text{ W/m}^3$ . At the same power input, adding 10% ring media class into BCR enhanced the  $K_L a$  coefficient performance about 16.4%–39.2% compared to the no media addition condition, while 16.9%–38.5% was improved by adding 10% cylinder media into ALR.

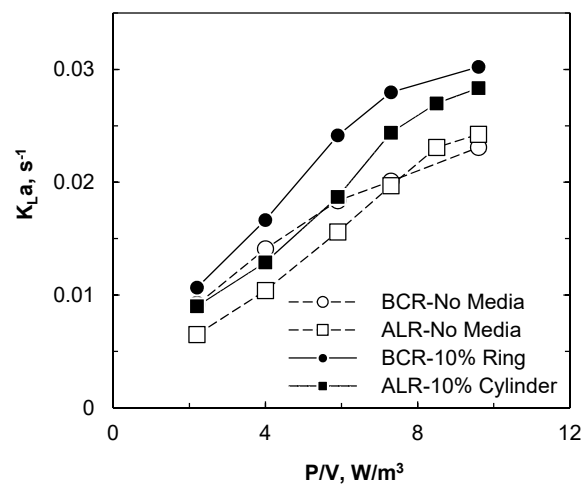


**Figure 10.** The effect of power consumption per unit volume ( $P/V$ ) on the  $K_L a$  coefficient comparing between non-addition media and ring media addition in BCR and cylinder media addition in ALR at 10% solid loading.

This  $K_L a$  value improvement is comparable with various existing research, including the study of Bun et al. [3] which enhanced the  $K_L a$  value in ALR from 6 to 28% by inserting slanted baffle in riser compartment. Tsuyoshi Imai and Hua Zhu [28] were also able to enhance the  $K_L a$  coefficient by about 6%–14% by providing the liquid-film-forming apparatus (LFFA). Plus, Zhiyong Zheng et al. [25] improved  $K_L a$  value by installing helical sieve plate, while Nataša Lj. Lukić [9] added self-agitated impellers for better  $K_L a$  performance.

#### 4. Conclusions

This study aimed to investigate the relative effect of various types of plastic solid media on the bubble hydrodynamic characteristics for improving oxygen mass transfer performance in both BCR and ALR. Four different types of solid polypropylene particle media, i.e., ring, sphere, cylinder, and square, were selected for this assessment. Bubble size ( $D_B$ ), bubble rising ( $U_B$ ), and specific interfacial area ( $a$ ) were analyzed in different superficial gas velocities to understand the internal mechanism of bubble hydrodynamics after adding solid media before estimating the oxygen mass transfer performance. The experimental result can be summarized as the following:

- A larger  $D_B$  was observed at higher  $V_g$ , regardless of additional media types, due to the promotion of bubble coalesce at higher airflow. Smaller bubbles, about 22%–27% and 5%–29% on average, were obtained after adding solid media in BCR and ALR, respectively, compared to the case without media addition due to the higher breaking rate over coalescence rate. Ring and cylinder media have a significant effect, resulting in smaller air bubbles, among the four media types investigated.
- Providing plastic media resulted in a slower bubble rising velocity in both reactors due to the decrease of liquid velocity caused by the increase of flow resistance and the ability of bubble capturing from free rising after adding solid media. The slowest bubble rising velocity was also observed from ring and cylinder additions. Consequently, the ring media added into BCR provided the highest bubble interfacial area, regardless of  $V_g$ , media types, and solid loading percentage. In ALR, cylinder media showed the maximum interfacial area at 5% loading, while cylinder and ring media became the most significant ones at 10%–15% solid loading.
- Up to 56% and 39%  $K_L a$  coefficient improvements were achieved after supplying solid media into BCR and ALR, respectively, compared to the non-addition case. The ring and cylinder solid media were defined as the most significant media for improving  $K_L a$  value in BCR and ALR, respectively, among the media examined without extra energy. At certain power input, adding 10% ring media in BCR, improved  $K_L a$  value up to 39% compared to no media addition, while up to 39% was improved after adding 10% cylinder media in ALR.

In conclusion, adding solid media into multi-phase reactors can improve the bubble hydrodynamic characteristics compared to the free media reactors through the capacity to reduce and/or maintain the bubble size distribution in the system as well as increase the bubble retention time in the reactors by decreasing bubble rising velocity. Smaller bubbles and a higher bubble retention time after adding solid media enlarged the specific bubble interfacial area, especially for the ring and cylinder media classes. This bubble hydrodynamic improvement resulted in the enhancement of the oxygen mass transfer coefficient ( $K_L a$ ) in both BCR and ALR without any additional power input. This finding is necessary for the systems requiring high oxygen transfer performance in chemical or biological processes.

**Author Contributions:** Conceptualization, P.S., S.B., K.W. and P.P.; Methodology, P.S. and K.W.; Formal Analysis, P.S. and S.B.; Investigation, P.S., S.B. and K.W.; Writing—Original Draft Preparation, P.S. and S.B.; Writing—Review & Editing, S.B., K.W., N.C., M.F. and P.P.; Supervision, N.C., M.F. and P.P. All authors have read and agreed to the published version of the manuscript.

**Funding:** This research work was supported by Department of Environmental Engineering, Faculty of Engineering, Chulalongkorn University, Thailand and the Center of Excellence on Hazardous Substance Management (HSM). It also has been partially supported by the Research Network NANOTECH (RNN) program of the National Nanotechnology Center (NANOTEC), NSTDA, Ministry of Science and Technology, Thailand.

**Acknowledgments:** Authors gratefully acknowledge faculty members, laboratory staffs and students in Environmental Engineering of Chulalongkorn University. Saret Bun also would like to acknowledge JICA Research Grant for Laboratory-Based Education (LBE) Project in Institute of Technology of Cambodia (ITC) for the research support during working on this manuscript.

**Conflicts of Interest:** The authors declare no conflict of interest.

## References

1. Couvert, A.; Roustan, M.; Chatellier, P. Two-phase hydrodynamic study of a rectangular air-lift loop reactor with an internal baffle. *Chem. Eng. Sci.* **1999**, *54*, 5245–5252. [[CrossRef](#)]
2. Yu, W.; Wang, T.; Liu, M.; Wang, Z. Bubble circulation regimes in a multi-stage internal-loop airlift reactor. *Chem. Eng. J.* **2008**, *142*, 301–308. [[CrossRef](#)]
3. Bun, S.; Wongwailikhit, K.; Chawaloeshonsiya, N.; Lohwacharin, J.; Ham, P.; Painmanakul, P. Development of modified airlift reactor (MALR) for improving oxygen transfer: Optimize design and operation condition using ‘design of experiment’ methodology. *Environ. Technol.* **2019**, 1–13. [[CrossRef](#)] [[PubMed](#)]
4. Bun, S.; Chawaloeshonsiya, N.; Nakajima, F.; Tobino, T.; Painmanakul, P. Comparative study of local gas-liquid hydrodynamics and mass transfer between conventional and modified airlift reactors. *J. Environ. Chem. Eng.* **2019**, *7*, 103206. [[CrossRef](#)]
5. Bun, S.; Chawaloeshonsiya, N.; Ham, P.; Wongwailikhit, K.; Chaiwiwatworakul, P.; Painmanakul, P. Experimental and empirical investigation of mass transfer enhancement in multi-scale modified airlift reactors. *Multiscale Multidiscip. Model. Exp. Des.* **2019**, 1–13. [[CrossRef](#)]
6. Luo, L.; Yuan, J.; Xie, P.; Sun, J.; Guo, W. Hydrodynamics and mass transfer characteristics in an internal loop airlift reactor with sieve plates. *Chem. Eng. Res. Des.* **2013**, *91*, 2377–2388. [[CrossRef](#)]
7. Nikakhtari, H.; Hill, G.A. Enhanced oxygen mass transfer in an external loop airlift bioreactor using a packed bed. *Ind. Eng. Chem. Res.* **2005**, *44*, 1067–1072. [[CrossRef](#)]
8. Lukić, N.L.; Šijački, I.M.; Kojić, P.S.; Popović, S.S.; Tekić, M.N.; Petrović, D.L. Enhanced hydrodynamics in a novel external-loop airlift reactor with self-agitated impellers. *J. Taiwan Inst. Chem. Eng.* **2016**, *68*, 40–50. [[CrossRef](#)]
9. Lukić, N.L.; Šijački, I.M.; Kojić, P.S.; Popović, S.S.; Tekić, M.N.; Petrović, D.L. Enhanced mass transfer in a novel external-loop airlift reactor with self-agitated impellers. *Biochem. Eng. J.* **2017**, *118*, 53–63. [[CrossRef](#)]
10. Moustiri, S.; Hebrard, G.; Roustan, M. Effect of a new high porosity packing on hydrodynamics of bubble columns. *Chem. Eng. Process. Process Intensif.* **2002**, *41*, 419–426. [[CrossRef](#)]
11. Bhatia, B.; Nigam, K.; Auban, D.; Hebrard, G. Effect of a new high porosity packing on hydrodynamics and mass transfer in bubble columns. *Chem. Eng. Process. Process Intensif.* **2004**, *43*, 1371–1380. [[CrossRef](#)]
12. Maldonado, J.G.; Bastoul, D.; Baig, S.; Roustan, M.; Hébrard, G. Effect of solid characteristics on hydrodynamic and mass transfer in a fixed bed reactor operating in co-current gas-liquid up flow. *Chem. Eng. Process. Process Intensif.* **2008**, *47*, 1190–1200. [[CrossRef](#)]
13. Wongwailikhit, K.; Warunyuwong, P.; Chawaloeshonsiya, N.; Dietrich, N.; Hébrard, G.; Painmanakul, P. Gas Sparger orifice sizes and solid particle characteristics in a bubble column—relative effect on hydrodynamics and mass transfer. *Chem. Eng. Technol.* **2018**, *41*, 461–468. [[CrossRef](#)]
14. Xue, T.; Liu, X.; Jin, Y.; Wu, B. Bubbles image processing and parameters measurement based on the high-speed photography. In Proceedings of the Seventh International Symposium on Precision Engineering Measurements and Instrumentation, Yunnan, China, 15 November 2011; p. 83210T.
15. Painmanakul, P.; Loubière, K.; Hébrard, G.; Mietton-Peuchot, M.; Roustan, M. Effect of surfactants on liquid-side mass transfer coefficients. *Chem. Eng. Sci.* **2005**, *60*, 6480–6491. [[CrossRef](#)]
16. Garcia, H.E.; Gordon, L.I. Oxygen solubility in seawater: Better fitting equations. *Limnol. Oceanogr.* **1992**, *37*, 1307–1312. [[CrossRef](#)]
17. Bouaifi, M.; Hebrard, G.; Bastoul, D.; Roustan, M. A comparative study of gas hold-up, bubble size, interfacial area and mass transfer coefficients in stirred gas-liquid reactors and bubble columns. *Chem. Eng. Process. Process Intensif.* **2001**, *40*, 97–111. [[CrossRef](#)]
18. Kim, S.-D.; Jang, H.-S. Hydrodynamics and bubble breakage in three phase fluidized beds. *Korean Chem. Eng. Res.* **1979**, *17*, 407–418.
19. Sarhan, A.; Naser, J.; Brooks, G. Effects of particle size and concentration on bubble coalescence and froth formation in a slurry bubble column. *Particuology* **2018**, *36*, 82–95. [[CrossRef](#)]
20. Livingston, A.; Zhang, S. Hydrodynamic behaviour of three-phase (gas-liquid-solid) airlift reactors. *Chem. Eng. Sci.* **1993**, *48*, 1641–1654. [[CrossRef](#)]
21. Zhang, T.; Wang, J.; Luo, Z.; Jin, Y. Multiphase flow characteristics of a novel internal-loop airlift reactor. *Chem. Eng. J.* **2005**, *109*, 115–122. [[CrossRef](#)]

22. Al Ba'ba'a, H.B.; Amano, R.S. A study of optimum aeration efficiency of a lab-scale air-diffused system. *Water Environ. J.* **2017**, *31*, 432–439. [[CrossRef](#)]
23. Sastaravet, P.; Chuenchaem, C.; Thaphet, N.; Chawaloesphonsiya, N.; Painmanakul, P.; Sastaravet, P.; Chuenchaem, C.; Thaphet, N.; Chawaloesphonsiya, N.; Painmanakul, P. Comparative study of mass transfer and bubble hydrodynamic parameters in bubble column reactor: Physical configurations and operating conditions. *Environ. Eng. Res.* **2014**, *19*, 345–354. [[CrossRef](#)]
24. Oliveira, M.S.; Ni, X.-W. Effect of hydrodynamics on mass transfer in a gas–liquid oscillatory baffled column. *Chem. Eng. J.* **2004**, *99*, 59–68. [[CrossRef](#)]
25. Zheng, Z.; Chen, Y.; Zhan, X.; Gao, M.; Wang, Z. Mass transfer intensification in a novel airlift reactor assembly with helical sieve plates. *Chem. Eng. J.* **2018**, *342*, 61–70. [[CrossRef](#)]
26. Yang, T.; Geng, S.; Yang, C.; Huang, Q. Hydrodynamics and mass transfer in an internal airlift slurry reactor for process intensification. *Chem. Eng. Sci.* **2018**, *184*, 126–133. [[CrossRef](#)]
27. Ferreira, A.; Ferreira, C.; Teixeira, J.; Rocha, F. Temperature and solid properties effects on gas–liquid mass transfer. *Chem. Eng. J.* **2010**, *162*, 743–752. [[CrossRef](#)]
28. Imai, T.; Zhu, H. *Improvement of Oxygen Transfer Efficiency in Diffused Aeration Systems Using Liquid-Film-Forming Apparatus*; InTech: Rijeka, Croatia, 2011.



© 2020 by the authors. Licensee MDPI, Basel, Switzerland. This article is an open access article distributed under the terms and conditions of the Creative Commons Attribution (CC BY) license (<http://creativecommons.org/licenses/by/4.0/>).